A Rugged Energy Landscape Mechanism for Trapping of Transmembrane Receptors during Endocytosis†

Stuart S. Licht,[§,‡,||] Alois Sonnleitner,[§,⊥,@] Shimon Weiss,[⊥,#] and Peter G. Schultz*[,‡,+]

Department of Chemistry, The Scripps Research Institute, La Jolla, California 92037, Division of Materials Science, Lawrence Berkeley National Laboratory, Berkeley, California 94720, Department of Chemistry and Biochemistry and Department of Physiology, University of California at Los Angeles, Los Angeles, California 90024, and Genomics Institute of the Novartis Research Foundation, San Diego, California 92121

Received May 7, 2002; Revised Manuscript Received October 21, 2002

ABSTRACT: Efficient clathrin-mediated endocytosis of transmembrane receptors requires that clathrin-coated pits retain the receptors long enough to allow vesicle formation and internalization. In many cases, however, the receptors can exhibit mean lifetimes in coated pits much shorter than the lifetime of the pit at the plasma membrane. A rugged energy landscape for binding, which produces a broad distribution of residence times, ensures a significant probability of times much greater than the mean and would allow efficient trapping of proteins in these cases. We used fluorescence correlation spectroscopy and total internal reflection microscopy to measure the kinetics of movement of a C5a receptor−yellow fluorescent protein fusion in living cells. These experiments demonstrate that clusters of trapped receptors exhibit fluctuations in fluorescence intensity that vary in time scale over 2 orders of magnitude. Most of the variation in intensity is likely due to the motion of the receptors in the plane of the plasma membrane, although it is not possible to rule out a small contribution from motion orthogonal to the plane of the membrane. The broad time scale distribution of the intensity fluctuations is consistent with a rugged energy landscape mechanism for trapping of the receptors. This mechanism, which allows efficient trapping to coexist with rapid exchange, may also be relevant to other biological processes involving binding in heterogeneous chemical environments.

Clathrin-mediated endocytosis is one mechanism by which eukaryotic cells modulate the activity of cell surface receptors (*1*, *2*). This process begins with targeting of the protein clathrin from the cytosol to the cell membrane, where it forms curved lattices called clathrin-coated pits. Transmembrane receptors that are targeted for internalization become concentrated in these pits, and internalization takes place through the action of dynamin, which assists in causing the clathrin-coated membrane to invaginate and form a vesicle. One issue of particular biological interest is how receptors become selectively concentrated in coated pits. In the case of G protein-coupled receptors (GPCRs),[1] phosphorylation of the receptor causes it to bind β-arrestin, which then can bind to both clathrin and the adaptor protein AP-2. The binding interactions between the receptor and coated pit component proteins such as clathrin and AP-2 allow discrimination between cargo and noncargo proteins.

Previous work has addressed some of the kinetic aspects of receptor trapping. The rate constant for coated pit internalization is typically ∼1 min^{-1} (*3*, *4*), while rate constants for receptor internalization are typically <0.5 min^{-1} (*5*−*7*). However, given the typical densities of coated pits [∼0.3 pits/μm^2 at 37 °C (*8*)] and the typical diffusion coefficients for membrane proteins [∼0.001−1 $\mu m^2/s$ (*9*, *10*)], rate constants of encounters of receptors with pits can be predicted to be much larger (∼3−300 min^{-1}) than those for either pit internalization or receptor endocytosis (*11*). Together, these observations argue that the probability is small that an encounter between a cargo molecule and a coated pit will be productive (that is, that the cargo will enter the pit and not dissociate from it before the pit is internalized).

† This work was supported by the grants from the National Institutes of Health (1R01GM063014-01), the Laboratory Directed Research and Development Program of Lawrence Berkeley National Laboratory under the U.S. Department of Energy (DE-AC03-76SF00098), the Molecular Design Institute of the Office of Naval Research (N0001498F0402), the Cancer Research Fund of the Damon Runyon-Walter Winchell Foundation (to S.S.L.), and the Erwin Schrödinger Foundation of Austria (to A.S.).

* To whom correspondence should be addressed. Telephone: (858) 784-9300. E-mail: schultz@scripps.edu.

‡ The Scripps Research Institute.

§ These authors contributed equally to this work.

|| Present address: Department of Chemistry, Massachusetts Institute of Technology, Cambridge, MA 02139.

⊥ Lawrence Berkeley National Laboratories.

@ Present address: Zentrum Biomedizinische Nanotechnologie, Upper Austrian Research, Austria.

University of California at Los Angeles.

+ Genomics Institute of the Novartis Research Foundation.

[1] Abbreviations: C5aR, C5a receptor; C5aR−EYFP, C5a receptor-enhanced yellow fluorescent protein fusion; FCS, fluorescence correlation spectroscopy; DFA, detrended fluctuation analysis; fwhm, full width at half-maximum; GPCR, G protein-coupled receptor; pdf, probability density function; TIR, total internal reflection; SEM, standard error of the mean.

10.1021/bi026059v CCC: $25.00
Published on Web 02/20/2003

Supporting the idea of a low probability of productive cargo−pit encounters, photobleaching recovery experiments have shown that several (*9*, *12*, *13*) [but not all (*14*, *15*)] receptors interact only transiently with coated pits during endocytosis. For asialoglycoprotein receptors, for example, the average lifetime in the coated pit can be estimated to be <2 s (*12*). However, using this lifetime to calculate a probability that a receptor in a coated pit fails to dissociate before internalization of the pit predicts an endocytotic rate constant that is ∼10-fold smaller than that observed.

One possible explanation for this discrepancy would be a process by which targeted receptors could increase the probability of vesiculation of a coated pit. A recent report suggests that in some cases, the presence of targeted receptors in coated pits can recruit endophilin (*16*), potentially increasing the probability of endocytosis for pits containing targeted receptors (*17*, *18*). Recruitment of endophilin could be a mechanism for improving both the efficiency and selectivity in the internalization of targeted receptors, depending on how much the presence of targeted receptor decreased the lifetime of a coated pit on the plasma membrane.

Another resolution of this problem would be a mechanism of receptor trapping that combines a short mean lifetime in the trap with a sufficiently high probability of a long trapped lifetime to allow efficient trapping. One mechanism having this characteristic is inspired by an analogy between endocytotic cargo trapping and charge transport in amorphous semiconductors. This charge transport has been modeled as an escape of electrons from energy wells of broadly distributed depths (*19*). The theory indicates that a broad distribution of well depths leads to lifetimes much greater than the mean being more common than would be expected for a uniform well depth (*19*, *20*). Mathematically, the broad distribution gives rise to a stretched exponential probability density function (pdf) for electron escape [i.e., $f(t) \propto \exp(t/\tau)^{\beta}$, with $\beta < 1$], as opposed to the exponential pdf [i.e., $f(t) \propto \exp(t/\tau)$] for a uniform well depth (*19*, *20*). Broad distributions of trapping times have also been proposed for diffusion in biological systems (*21*). In the context of endocytosis, a mechanism analogous to this charge transport mechanism would postulate a rugged energy landscape for the receptor−pit interaction (with rugged energy landscape here meaning a broad distribution of binding energies). Conformational heterogeneity in the protein and membrane components of the coated pits could produce an energy landscape for binding in which both shallow energy wells (weak binding) and deep energy wells (strong binding) are accessible, leading to a broad distribution of trapping times. Increasing the breadth of a distribution of binding energies would be expected to increase the efficiency of trapping of a substrate protein, and a difference in the breadths of distributions between a correctly targeted protein and an incorrectly targeted one would give rise to selective trapping. The Appendix contains a quantitative discussion of these mechanisms for a highly simplified model.

Here we have used fluorescence correlation spectroscopy (FCS) and total internal reflection (TIR) microscopy (*22*) to investigate the kinetics of the motions that a GPCR (fused to the yellow fluorescent protein) undergoes during endocytosis. The GPCR we have studied, the C5a receptor, is known to be endocytosed in response to its agonist, the complement component C5a (*23*, *24*). The results are consistent with a heterogeneous energy landscape for interaction of the C5a receptor with immobile cell components.

MATERIALS AND METHODS

Materials. C5a (recombinant) was obtained from Sigma.

Plasmid Construction. The pC5aR-EYFPN3 plasmid was derived from pC5aR-EGFPN3 (*25*). The 0.7 kb fragment encoding EYFP was amplified from pEYFP (Clontech), using primers that introduced *Bam*HI and *Not*I sites at the 5′ and 3′ ends, respectively. This fragment was cloned into pC5aR-EGFPN3 between the *Bam*HI and *Not*I sites, replacing the fragment encoding EGFP with the EYFP fragment.

Cell Culture and Transfection. HEK-293 cells were grown on DMEM supplemented with 10% fetal bovine serum. Cultures at 75−95% confluency were plated onto coverslips (either standard glass for FCS experiments with the 1.4 NA objective or Olympus glass for TIR experiments with the 1.65 NA objective) that had been sonicated in potassium hydroxide (1 h for standard glass and 2 h for Olympus glass) and thoroughly rinsed in PBS. The cells were transfected 12−24 h after plating using Fugene-6 (Roche) according to the manufacturer's instructions. One well of a standard six-well plate was typically transfected using 5 ng of pC5aR-EYFPN3. The plasmid DNA was diluted with salmon sperm DNA (Sigma) so that the total amount of DNA added was 1 μg. Fluorescence experiments were carried out 12−48 h after transfection. Immediately before imaging experiments were carried out, cells were washed with PBS and placed into Ringer's solution [118 mM NaCl, 4.7 mM KCl, 1.2 mM $MgSO_4$, 4.2 mM $NaHCO_3$, 1.3 mM $CaCl_2$, and 10 mM HEPES (pH 7.4)].

For potassium depletion experiments (*26*), the cells were rinsed with potassium-free Ringer's solution [118 mM NaCl, 1.2 mM $MgSO_4$, 4.2 mM $NaHCO_3$, 1.3 mM $CaCl_2$, and 10 mM HEPES (pH 7.4)]. The cells were then incubated in a hypotonic solution (1:1 potassium-free Ringer's/Millipore water mixture) for 5 min, rinsed in potassium-free Ringer's solution, and incubated in potassium-free Ringer's solution for 30 min.

Fluorescence Correlation Spectroscopy. The cells were put in a temperature-controlled perfusion cell and kept at 37 °C in Ringer's solution (see above). The beam of an argon ion laser (514 nm) was tightly focused onto the basal or apical membrane of the cell at a power of 2−10 μW, with most experiments performed at 5 μW. The size of the illuminated spot was calibrated using the known diffusion coefficient of rhodamine 6G; this measurement agreed with the size measured by imaging of the spot on a CCD camera. The spot size was observed to be independent of whether the focal plane was at the basal or the apical surface of the cell, and diffusion times were identical for the two surfaces, indicating that passage of the light through the cell did not affect the spot size. Diffusion times were also independent of laser intensity for values of <10 μW. To correct for uncorrelated afterpulsing of photodiode detectors, the fluorescence was split with a nonpolarizing beam splitter cube and collected onto two avalanche photodiodes, producing a pulse for every photon arriving. The pulses were collected with a counting board and subjected to software cross correlation. The fitting was carried out in Origin 6.0 (OriginLab). The quality of the fit was determined by visual

comparison of the residuals of the fits for different fitting models. We compared the following models with the corresponding autocorrelation functions G: (1) two dark states with one diffusing species in which $G = G_0 + N^{-1}\{1 + [F_1/(1 - F_1)\exp(-t/\tau_{d1})]\}\{1 + [F_2/(1 - F_2)\exp(-t/\tau_{d2})]\}[1 + (t/\tau_D)]^{-1}$; (2) two dark states with two diffusing species in which $G = G_0 + N^{-1}\{1 + [F_1/(1 - F_1)\exp(-t/\tau_{d1})]\}\{1 + [F_2/(1 - F_2)\exp(-t/\tau_{d2})]\}\{Y_1[1 + (t/\tau_{D1})]^{-1} + Y_2[1 + (t/\tau_{D2})]^{-1}\}$; and (3) two dark states with anomalous diffusion in which $G = G_0 + N^{-1}\{1 + [F_1/(1 - F_1)\exp(-t/\tau_{d1})]\}\{1 + [F_2/(1 - F_2)\exp(-t/\tau_{d2})]\}[1 + \Gamma(t^{\alpha}/w^2)]^{-1}$ (see also ref *27*). In all the models, two dark states were used according to reports of the presence of two dark states in EGFP (*28*) with the observed characteristic times being similar to those reported previously (*28*). One diffusing species was assumed to be the C5aR−EYFP protein in the membrane before agonist addition. After agonist addition, we assumed that clustering or other biochemical changes took place such that there would now be two diffusing species in the membrane: the C5aR−EYFP protein and clusters of the C5aR−EYFP protein which would have different diffusion times (perhaps because of binding to immobile cell components). This model proved to be insufficient to explain the observed autocorrelation data; we therefore introduced the anomalous diffusion model, which takes a range of interactions into account.

Total Internal Reflection Fluorescence Microscopy (TIRFM). Fluorescence detection and excitation were performed using a Zeiss Axiovert microscope. The beam of a 100 mW argon ion (514 nm) laser (Melles Griot) was reflected off of a 527DRLP dichroic (Omega) and focused at the back focal plane of an Apo 100 × 1.65 NA oil/∞ objective (Olympus) so that it emerged into the immersion oil at an angle shallower than the critical angle θ_c, but close to the maximum angle of emergence for a very thin illumination layer. $\theta_c = \sin^{-1}(n_1/n_2) \approx 50°$, where n_1 is the cytosol refractive index (1.37) and n_2 is the coverslip refractive index (1.78, Olympus) (*29*−*31*). The maximum angle of emergence θ is given by the equation $\theta = \sin^{-1}(\mathrm{NA}/n_2) \approx 68°$, where NA is the numerical aperture of the objective (1.65). Under these conditions, illumination generated an evanescent field of excitation decaying exponentially from the glass−buffer interface into the buffer (decay length to $1/e$ in ∼50 nm). The exciting spot was 15−25 nm in diameter. Excitation powers ranged from 80 to 500 μW. Fluorescent emission was filtered with a 535/30 band-pass filter (Omega), and reflected laser light was excluded with a 514 nm notch filter (Kaiser). Detection was carried out with a Pentamax GenIV intensified camera at an intensifier setting of 80%. Images were usually recorded in the 2 × 2 hardware binned mode, which yields a pixel size in the image plane of 225 nm.

Analysis of Images. Clusters of fluorophore that did not change position over the course of the recording were visually identified. Mobile clusters (which are likely to represent the C5aR−EYFP fusion in clathrin-coated vesicles, rather than coated pits) were not used for this analysis. Time series of cluster intensities were generated using the WinView imaging software. To determine the relationship between intensity changes and changes in the width of the intensity distribution, we fit the image of the cluster to a two-dimensional Gaussian. A 15 × 15 pixel area centered on the cluster (approximate size of ∼2 and ∼8 pixels for binned and unbinned data, respectively) was fit. We extracted

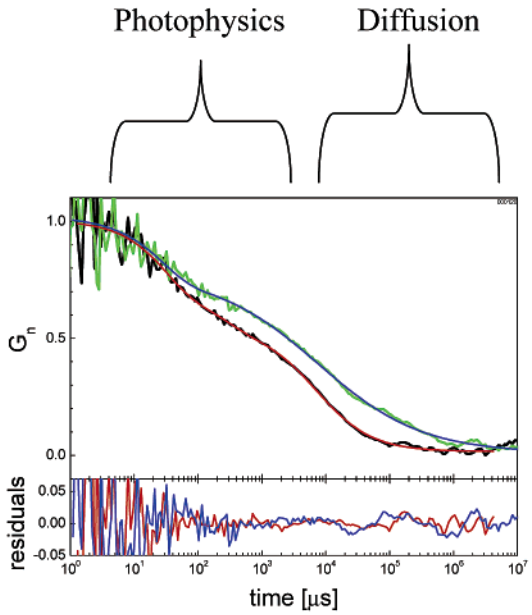

FIGURE 1: Fluorescence correlation spectroscopic traces from HEK-293 cells expressing the C5aR−EYFP protein. The black trace was recorded before the addition of agonist, while the green trace was recorded ∼5 min after perfusion of Ringer's solution containing 10 nM C5a over the cell. The black trace has been fit to a model with one triplet time and one diffusion time, while the green trace has been fit to a model with one triplet time and two diffusion times.

the full width at half-maximal intensity (fwhm) from the Levenberg−Marquardt fit of each frame. The mean of the fwhm along the axes of the two-dimensional Gaussian was plotted as a function of the peak intensity. Simulations suggest that the fitting procedure is accurate when the peak intensity is as low as 2σ of the background noise; the experimental peak intensities were this large or larger. To assess the degree of correlation between intensity changes and changes in fwhm, we calculated the differential changes in intensity and fwhm and performed a cross-correlation analysis. The analysis was carried out in LabView (National Instruments).

Detrended Fluctuation Analysis. The program dfa was obtained from the Margaret and H. A. Rey Laboratory for Nonlinear Dynamics in Medicine (http://reylab.bidmc.harvard.edu/). This program performs detrended fluctuation analysis (DFA) (*32*−*35*) on time series data. First, the data are divided into blocks of length n. A linear fit to the data in each block defines the "trend". This trend is subtracted from the data in the block. The variance of the detrended data is calculated for each block. From these variances, a mean variance for a given block length is determined. The mean variance is plotted against the block length as a log−log plot. The slope of this plot is called α. The α parameter in DFA is related to the power spectral density, $S(f)$,of the process (*34*, *36*):

$$\alpha = \frac{\beta + 1}{2} \text{ for a process with } S(f) \propto \frac{1}{f^{\beta}}$$

Thus, for white noise, $\beta = 0$ for the spectral density function and $\alpha = 0.5$. For a process with a characteristic correlation time (e.g., fluctuations associated with a single chemical equilibrium), the spectral density function exhibits a corner

frequency at the correlation time, where $\beta = 0$ at frequencies lower than the corner frequency and $\beta = 2$ at high frequencies (*37*). In DFA, this would manifest itself as a crossover from $\alpha = 0.5$ to $\alpha = 1.5$. If the data exhibit power law correlations, $0 < \beta \leq 1$ and $0.5 < \alpha \leq 1$, with the case of $\beta = \alpha = 1$ corresponding to the special case of $1/f$ noise. Thus, DFA, like power spectral density analysis, provides a method for determining the characteristic time scales of fluctuations, and the two methods perform comparably as estimators for the exponents of power law statistics (*36*).

Detrended fluctuation analysis was carried out on time series of normalized intensity, i.e., the intensity of a small region of interest divided by the intensity of a large area (>75%) of the entire cell. This procedure normalizes for the effects of photobleaching and fluctuations in laser power intensity. Detrended fluctuation analysis was carried out on time series consisting of 2000 normalized intensities derived from images recorded 100 ms apart.

RESULTS

Diffusional Dynamics of the C5a Receptor. To address the kinetics of the interaction of C5a with immobile cell components during endocytosis, the diffusional dynamics of a C5a receptor−yellow fluorescent protein fusion (C5aR−EYFP) in live HEK-293 cells were probed using FCS (*38*). In the absence of C5a, the FCS trace observed in cells expressing the C5aR−EYFP fusion (Figure 1, black trace) is fitted well by a model which includes components from the dark states (*28*) of the EYFP fluorophore (the short time scale feature) and from normal (i.e., Fickian) diffusion (the long time scale feature). This model gives a diffusion coefficient of $4.4 \pm 2.4\ \mu m^2/s$ for the C5aR−EYFP fusion, which is consistent with unhindered diffusion of a transmembrane protein (*10*, *39*). The diffusion coefficient measured from the top and bottom (adherent) surfaces of cells is the same (data not shown).

Application of the agonist C5a at saturating concentrations (10 nM) (*40*) caused a dramatic change in the diffusional behavior of the C5aR−EYFP protein. In 56% of observations, application of C5a caused the apparent diffusion coefficient of the C5aR−EYFP protein to decrease significantly (Figure 1, green trace), as judged by the characteristic time of autocorrelation decay in the FCS trace. The short correlation time corresponding to the photophysics of EYFP was not affected by agonist treatment. Fitting FCS traces obtained either before or after addition of C5a to a normal diffusion model suggests that the diffusion coefficient decreases 2.7-fold on average. The time traces of fluorescence intensity (Figure 1 of the Supporting Information) indicate that increases in intensity manifest themselves as discrete events of homogeneous intensity, suggesting that fluctuations arise from the diffusion of individual receptors rather than from motion through a local concentration gradient or from motion of submicroscopic clusters.

Addition of the agonist also causes the FCS traces to exhibit a decay in autocorrelation more gradual than that observed in the absence of agonist. FCS data from C5a-treated cells are not well-fitted with the model that includes a single diffusion coefficient. Better fits are achieved with models that include two diffusion coefficients or anomalous diffusion, in which the diffusion coefficient is time-dependent

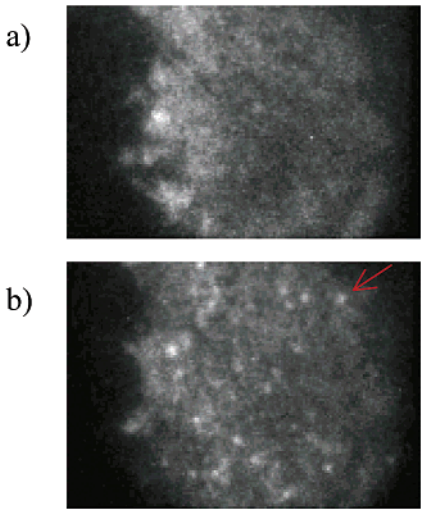

FIGURE 2: C5aR−EYFP clusters form in response to perfusion of C5a (a) before addition of C5a and (b) 5 min after addition of 10 nM C5a. The red arrow points to a C5aR−EYFP cluster.

(*41*). The anomalous diffusion model provides the best fit, as judged by residuals (see Materials and Methods).

C5a Causes the C5aR−EYFP Protein To Assemble into Large Clusters. Total internal reflection (TIR) microscopic images of cells expressing the C5aR−EYFP protein (Figure 2a and Supporting Information) show the protein to be expressed more or less uniformly in the cell membrane before addition of the agonist, as expected. In addition, multiple images taken at a frame rate of $10\ s^{-1}$ show the receptor to be highly mobile. TIR images of C5aR−EYFP-expressing cells after the addition of C5a show a heterogeneous distribution of the C5aR−EYFP protein (Figure 2b). The C5aR−EYFP fusion assembles into large clusters (image sizes of $1-10\ \mu m^2$) in the membrane. These assemblies can persist for up to ~10 s and disappear as a unit in ≤100 ms. However, the C5aR−EYFP protein is also observed outside these assemblies, in what appears from time series of images (Supporting Information) to be a highly mobile state.

One possibility is that the clusters represent the C5aR−EYFP protein bound to clathrin-coated pits. Since potassium depletion of cells has been shown to disassemble clathrin-coated pits in vivo (*42*), the effect of this treatment on the clusters of the C5aR−EYFP fusion was investigated. Potassium depletion was observed to prevent the formation of these clusters, and to disrupt clusters that had already formed (data not shown).

Dynamics of C5aR−EYFP Clusters. Clusters of the C5aR−EYFP protein exhibited striking dynamic behavior: the fluorescence intensity of clusters was observed to change by up to 10-fold over the course of ~10 s (Figure 3a). A normalized intensity (see Materials and Methods) was determined in a region of interest containing a cluster for each frame of a time series of movies. This analysis was also carried out for small sections (4 pixels, or $0.2\ \mu m^2$) of the image containing no visually identifiable cluster (Figure 3b), and for sections of the image outside of the cell and containing no fluorophores (data not shown). While the intensity fluctuations observed in the absence of fluorophores (representing read noise of the CCD camera) and those observed for the nonclustered C5aR−EYFP protein appear to be uniform in amplitude over time, the intensity fluctua-

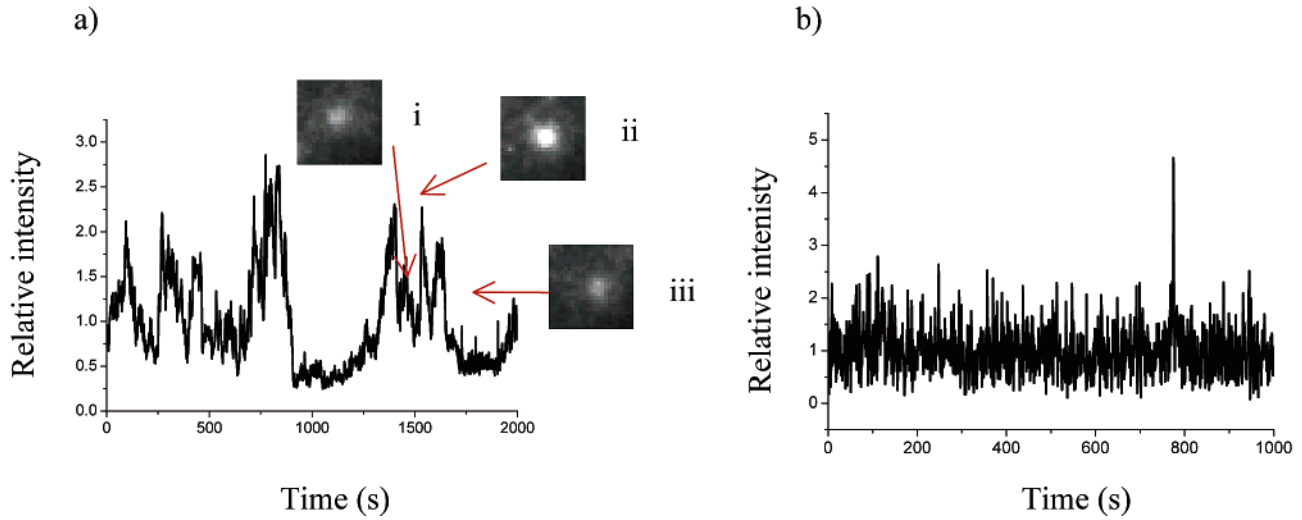

FIGURE 3: Intensity fluctuations in C5aR−EYFP clusters observed after addition of C5a. The normalized intensity was calculated as described in Materials and Methods; relative intensities presented here are normalized intensity/minimum normalized intensity in the recording. (a) Area of the cell containing a cluster. Insets are images of the cluster 132 (i), 154 (ii), and 168 s (iii) after the beginning of the recording. (b) Area of the cell with no cluster. The increased noise in panel b has its origin in the lower signal for noncluster areas, which will increase the noise for the intensity ratios.

tions of the C5aR−EYFP clusters appear to exhibit multiple characteristic time scales, with small fluctuations occurring on short time scales and large fluctuations occurring on longer time scales.

Many mathematical methods are available for the analysis of the kinetic characteristics of fluctuations in time series data; common ones include power spectral density function analysis and autocorrelation analysis. To address the question of the range of time scales over which intensity fluctuations occur in our experiments, we have chosen detrended fluctuation analysis (DFA) (*33*). This method tracks the amplitude of fluctuations in a given time window after subtraction of the global trend over that time window. DFA is convenient for our purposes because the slope (α) of a log−log plot of the amplitude of fluctuations (N) as a function of the time over which this amplitude is measured (n) provides information about the range of time scales over which fluctuations are correlated.

As judged by DFA, intensity fluctuations associated with the freely diffusing receptor exhibit correlation characteristics that differ from intensity fluctuations associated with the receptor in clusters. For data taken from cells before addition of C5a (Figure 4a), when the C5aR−EYFP protein diffuses freely, DFA gives an α of 0.6 ± 0.1 (SEM from 12 time series in four cells, data taken over 50 s), consistent with uncorrelated fluctuations. However, for data taken from visually identified clusters in cells that have been treated with C5a, α values significantly higher than 0.5 are observed. In some cases, the plot of log(n) versus log(N) is linear over the entire time range (corresponding to >2 orders of magnitude) (Figure 4b, red arrow). For these clusters, α equals 1.2 ± 0.1 (SEM from 13 time series in eight cells, data taken over 200 s).

In other cases, the plot is only linear over ~1 order of magnitude, with a transition between a lower α and a higher α evident at an intermediate time scale (Figure 4b, green arrow). The α values for these clusters are 0.76 ± 0.2 and 1.2 ± 0.2 (SEM from 16 time series in 11 cells, data taken over 200 s) in the limits of short and long times, respectively. However, DFA carried out in areas of C5a-treated cells that were well-separated (>2 μm) from clusters gave α values of 0.53 ± 0.04 (SEM from eight time series in six cells, data taken over 200 s), consistent with uncorrelated fluctuation. Spatial inhomogeneity also appears to contribute to the observed variation in α, as unclustered areas near (<2 μm) clusters gave α values of 0.6 ± 0.14 and 1.0 ± 0.2 (SEM of 14 time series in nine cells, data taken over 200 s) for short and long times, respectively.

Because the evanescent wave of the excitation light decays exponentially with distance from the glass surface in a TIR experiment, and because a cluster of fluorophores might be able to drift out of the focal plane of the microscope, intensity fluctuations might arise either from the fluctuation of the number of fluorophores in the area or from the motion of the fluorophores normal to the plane of the glass surface of the coverslip. To distinguish between these possibilities, the dependence of the width of the intensity distribution of a cluster on the total intensity of the cluster was investigated. For a cluster moving out of the focal plane, a decrease in total intensity would be correlated with an increase in the width of its intensity distribution. The widths of intensity distributions were estimated from the image data (see Materials and Methods) over the entire time series, and compared to the total intensities. The total intensity is either uncorrelated (Figure 5) or positively correlated (data not shown) with the width of distribution, suggesting that drift through the focal plane on length scales of >100 nm does not contribute significantly to the fluctuations. In addition, changes in intensity are uncorrelated with changes in the width of the distribution on the experimentally accessible time scales (Figure 5, inset).

Analysis of the distribution of intensities observed over time is another way of testing the idea that the intensity fluctuations arise from addition and removal of fluorophores from the cluster, rather than partial invagination of coated pits. The intensity distribution observed in our studies (Figure 6) has a peak at low relative intensity, and is skew toward higher intensities. If changes in intensity are due to motion

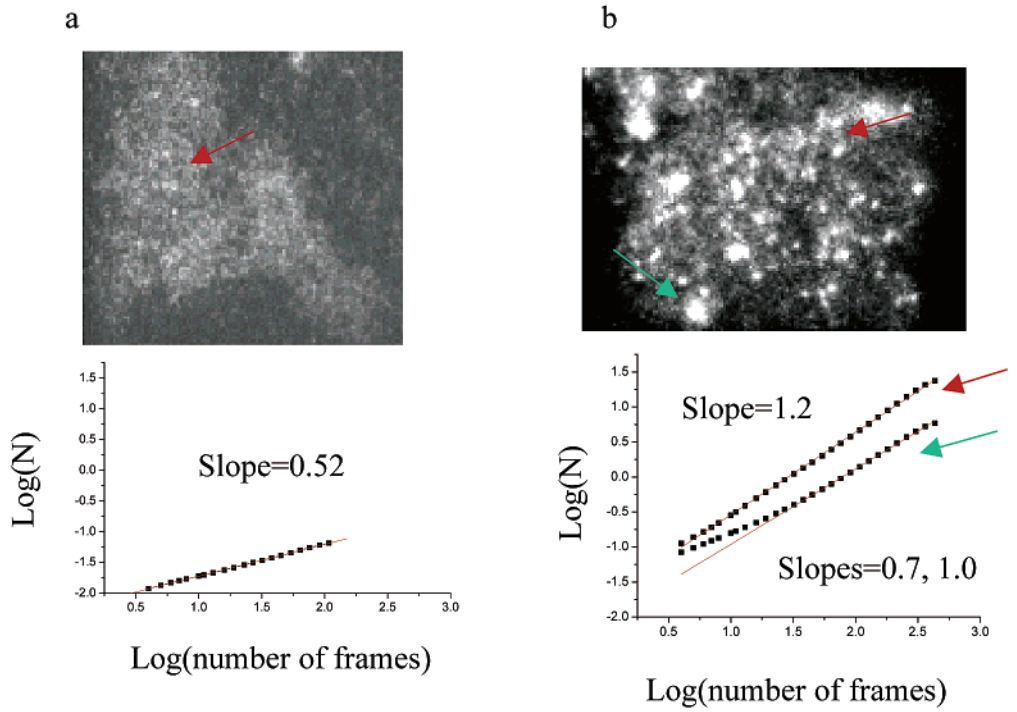

FIGURE 4: Detrended fluctuation analysis (DFA) for comparison of dynamics of the free and clustered C5aR−EYFP protein. Here *N* is the fluctuation amplitude of the normalized fluorescence intensity. (a) C5aR−EYFP in the absence of C5a (top) and DFA of the normalized intensity of a small (4 pixel) image area showing uncorrelated fluctuations (bottom). (b) C5aR−EYFP after addition of 10 nM C5a (top) and DFA of a cluster (red arrow) showing correlations with no characteristic time scale over 2 orders of magnitude (bottom). Another cluster (green arrow) has correlations over 1 order of magnitude, with correlated fluctuations at both short and long times.

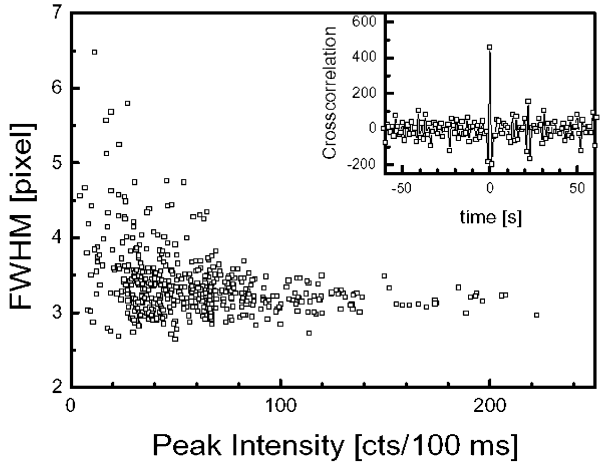

FIGURE 5: Full width at half-maximum (fwhm) of clusters and intensity of the cluster are uncorrelated. In the inset, the cross-correlation function of the fwhm and intensity shows that changes in these quantities are also uncorrelated; 1 pixel corresponds to 225 nm, i.e., the spots had a size of roughly 350 nm.

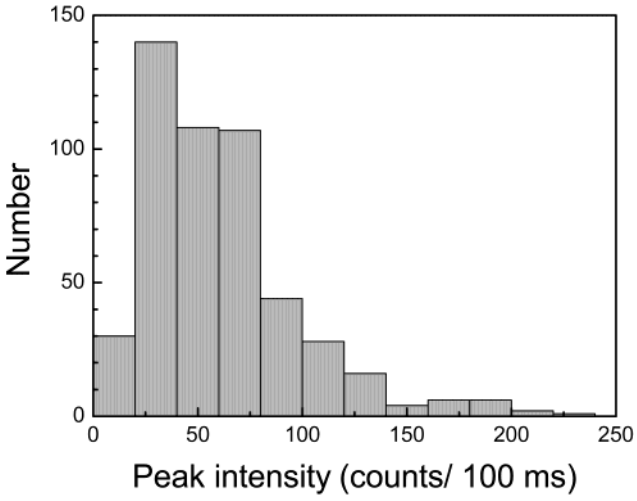

FIGURE 6: Distribution of intensities in an identified cluster measured over 200 s.

in the *z*-direction, this result would require coated pits to be most frequently observed in a deeply invaginated shape, in which the bulk of their cargo was shifted 100−200 nm from the surface of the membrane (*43*, *44*).

DISCUSSION

Diffusional Dynamics of the C5a Receptor. Efficient endocytosis through coated pits is straightforward if target receptors interact with the coated pits with a lifetime that is not much shorter than the lifetime of the pit at the plasma membrane [∼1 min (*3*, *4*)]. Evidence for this mechanism has been observed for the endocytosis of several receptors (*14*, *15*). Since both coated pits (*9*) and uncoated pits (*45*, *46*) are essentially immobile on the time scale of seconds, endocytosis through either pathway would require interaction of the mobile receptor with an immobile cell component. Fluorescence correlation spectroscopy can address the question of the lifetime of the receptor−pit interaction, an interaction that is long compared to the diffusion time of the unhindered receptor through the confocal spot will not influence the observed diffusion time, while an interaction with a lifetime comparable to the unhindered diffusion time will lead to a smaller observed diffusion coefficient (*47*). Thus, this technique is likely to be useful in determining whether the lifetime of the interaction of a given receptor

with coated pits is comparable to the lifetime of the pit at the cell surface or whether a more complex kinetic mechanism for endocytosis might be required.

The value of the diffusion coefficient of the C5aR−EYFP protein expressed in HEK-293 cells (4.4 ± 2.4 $\mu m^2/s$) in the absence of C5a is consistent with the hypothesis of unhindered Brownian motion of the C5aR−EYFP protein in the plasma membrane of cells under conditions that do not support endocytosis. The observation that treatment of C5aR−EYFP-expressing cells with a saturating concentration of C5a causes, on average, a >2-fold decrease in the observed diffusion coefficient supports the idea that this receptor interacts with immobile cell components with a mean lifetime of ~10 ms under conditions that support endocytosis. Thus, these experiments suggest that the simplest mechanism for endocytosis may not suffice to explain endocytosis of these receptors.

The hypothesis of a rugged energy landscape for receptor trapping would predict transient interaction of the receptor with an immobile cell component, with binding and unbinding characterized by multiple kinetic components. In the limit of a large number of bound states closely spaced in energy, anomalous diffusion of the receptor would be expected (*48*). The kinetics observed by FCS are consistent with the rugged energy landscape mechanism, as the FCS trace exhibits a minimum of two kinetic components and is best fitted with an anomalous diffusion model.

By themselves, however, the FCS data are subject to a number of ambiguities in interpretation. First, the effect of the agonist on the diffusional behavior of the C5aR−EYFP protein was highly variable among observations (diffusion times increased anywhere between 1.5- and 3.9-fold, and no effect was observed in 44% of the trials). One possible explanation for this variability comes from the fact that in these FCS experiments, the distance from the confocal spot from coated pits or other receptor traps is unknown. If the receptor interacts with traps that are distributed with a correlation length that is large compared to the size of the confocal spot, one could observe a range of diffusional behaviors depending on the distance of the confocal spot from the nearest traps.

In addition, the FCS data do not address the issue of the identity of the immobile cell component(s) with which the receptors interact. While many GPCRs have been shown to undergo endocytosis through clathrin-coated pits (*1*), a previous study has reported that the C5a receptor is endocytosed through a non-clathrin pathway, perhaps through caveolae (*49*). Interactions with cytoskeletal components or lipid rafts might also contribute to the observed mobility change.

Finally, the FCS analysis is relatively insensitive to the difference between a small number of kinetic components in diffusion and a large number of components. While the anomalous diffusion model provides the best fit, a model with two diffusion times also provides a reasonably good fit. The FCS data thus do not strongly distinguish between a small number of distinct binding interactions between the receptor and immobile cell components and a broad distribution of binding interactions of varying strength.

C5a Causes the C5aR−EYFP Protein To Assemble into Large Clusters. Imaging experiments were carried out to address some of the mechanistic questions left open by the FCS experiments. The observation of large clusters of C5a receptors in cells treated with C5a is consistent with the hypothesis that activation by the agonist causes the receptors to associate with an immobile cell component. The TIR images also show that between the clusters, the C5a receptor is diffusing rapidly (Supporting Information). This spatial heterogeneity in dynamics suggests that at least part of the high variability observed in the effect of C5a on the diffusion coefficient as observed by FCS is due to the fact that the confocal spot may sample different environments in different trials, with large effects seen close to a cluster and small effects seen further from a cluster.

The observation that these clusters can disappear within <100 ms suggests that the receptor−immobile component complex is transported into the cell interior, leading to the rapid disappearance of the cluster as it moves out of the TIR evanescent field. The ability of a potassium depletion treatment to prevent formation of receptor clusters and to disrupt clusters that had already been formed suggests that clathrin-coated pits are the immobile cell component to which the receptors are binding, since these structures are known to be sensitive to potassium depletion (*26*). Taken together, these observations are consistent with the hypothesis that the observed clusters are C5a receptors interacting with clathrin-coated pits that vesiculate and become internalized. The observation that dominant interfering mutants of clathrin, arrestin, and dynamin have minimal effects on the rate of endocytosis of C5aR (as measured by the amount of receptor internalized over the course of 45 min) (*49*) may reflect the nature of the rate-limiting step in C5aR endocytosis through the clathrin-mediated pathway, or may indicate that an alternate pathway can substitute efficiently for the clathrin-mediated pathway in cells expressing dominant negative mutants of coated pit components.

Dynamics of C5aR−EYFP Clusters. Measuring the fluorescence fluctuations of clusters in a time series of images provides a method for addressing the question of whether interactions of the receptor with the immobile cell component exhibit a characteristic time scale or a broad range of time scales. We chose DFA for analysis of these data. The fluctuation amplitude in DFA is analytically related to the power spectral density function through an integral transform, and the two methods of analysis perform comparably on stochastic signals (*36*). The slope (α) of the log−log plot relating the time scale of fluctuations (n) to the amplitude of fluctuations (N) can be interpreted in terms of the correlation characteristics of the fluctuations (*33*). For uncorrelated (white) noise, α is predicted to be 0.5, while for the Brownian noise associated with single processes (e.g., a single chemical equilibrium), α is predicted to be 1.5. Long time correlations are associated with $0.5 < \alpha < 1.5$; when $0.5 < \alpha < 1$, these long time correlations have the form of a power law. The special case of $\alpha = 1$ corresponds to $1/f$ noise. In DFA of these fluorescence fluctuations, transport in and out of coated pits with single on- and off-rates would manifest itself as a crossover in slope from $\alpha = 1.5$ (correlated fluctuations) to $\alpha = 0.5$ (uncorrelated fluctuations or "white noise") at a characteristic time determined by the rate of approach to equilibrium [analogous to current fluctuations arising from opening and closing of ion channels (*37*)]. The observation that many clusters exhibit an α of ≈ 1 with no apparent characteristic time is consistent with

transport in and out of the clusters taking place on time scales that vary over 2 orders of magnitude.

Some of the data for intensity fluctuations of clusters did exhibit crossovers, but in those cases, the slopes of the log(N) versus log(n) plots in the limit of long times did not tend toward 0.5, as would be expected for a process with a single characteristic time. For intensity fluctuations in areas of the image that are close to clusters, the reason for the crossover from uncorrelated to correlated fluctuations may be that the fluctuations at short times are due mostly to the unhindered diffusion of the receptor, while transport of receptor between the observed area and the nearby cluster takes place on a broad range of slower time scales. These data are thus consistent with the conclusion that the trapping of receptors in clathrin-coated pits exhibits a broad range of characteristic lifetimes (1−2 orders of magnitude), rather than the single characteristic time expected for a simple binding−unbinding equilibrium.

However, the process of binding and unbinding of receptors from an immobile cell component is not the only possible source of the observed fluorescence intensity fluctuations. Motion of the receptors in the z-direction (i.e., orthogonal to the plane of the coverslip) might also account for intensity fluctuations. From the depth of focus of the objective and the wavelength of illumination, it is possible to calculate a defocused image's expected full width at half-maximal intensity (fwhm), using the parabolic dependence of this quantity on the distance from the focal plane. If motion in the z-direction were the dominant source of the intensity fluctuations, the amplitude of the fluctuations (∼5-fold) would require motions of ∼100 nm, since the decay length of the evanescent field is 50 nm (assuming a refractive index for cytosol of 1.36−1.37) (*50*). In these experiments, a defocusing of 100 nm would increase the fwhm by ∼5%, while a defocusing of 300 nm would increase the fwhm by ∼30%. Estimating the resolution limit of our analysis as 0.1 pixel suggests that increases in the fwhm of ≥10% should be observable, making this method of analysis feasible as a diagnostic for intensity changes due to motion normal to the glass surface on length scales of >100 nm. These data are thus consistent with the hypothesis that intensity fluctuations in clusters arise mainly from addition and removal of fluorophores from the clusters. However, they do not rule out a contribution from motions of ≤100 nm, which could arise from partial invagination of coated pits.

The distribution of intensities in a time series provides a way of addressing the question of whether partial invagination of coated pits is contributing to the intensity fluctuations. Data from electron microscopy suggest that most clathrin-coated pits are shallow, rather than deeply invaginated (*44*, *51*). If most of the variance in cluster intensity was due to variance in pit geometry, the distribution of cluster intensities would be expected to have a peak at high relative intensity, representing the receptor clusters closest to the focal plane. In fact, the distribution has its peak at a low relative intensity (Figure 6). Therefore, while fluctations in the shape of the coated pit may contribute to the intensity fluctuations, they are not likely to be the dominant source of these fluctuations.

Since the fluctuations in intensity are likely to be associated with movement of receptors within the plane of the membrane, it is possible to interpret the correlation properties of these fluctuations in terms of the kinetics of cargo trapping. There are several plausible mechanisms that may contribute to the observed heterogeneity of trapping times. Subclustering of adaptor proteins (*2*, *52*) could introduce heterogeneity in the microenvironment of the coated pit. Energies of remodeling of the clathrin lattice structure have also been predicted to be approximately equal to kT (*53*), so a heterogeneous distribution of adaptor−receptor complexes might interact with a distribution of local lattice structures in the pit. Fluctuations in membrane curvature might have an effect on protein−protein interaction, which theoretical studies estimate to be approximately equal to kT (*54*). Since invaginated coated pits are known to form a constricted intermediate which is inaccessible to proteins added extracellularly (*44*, *55*), partial invagination of the pit, coupled to constriction of its neck, is likely to hinder diffusion of trapped receptors out of the pit. Finally, rate constant heterogeneity might also be due to the existence of multiple accessible energy minima and/or transition states in the energy surfaces for binding of receptors to coated pit components (*56*−*59*). Dispersions in rate constants due to slow conformational changes up to several orders of magnitude have been reported (*58*). Taken together, these factors could produce a rugged energy landscape for receptor−coated pit interactions, with free energies of interaction varying over the range several kT required to explain the observed broad distribution of time scales.

These studies have provided evidence that trapping of C5a receptors in clathrin-coated pits involves a broad distribution of trapping rate constants, rather than the single characteristic trapping time one might expect for a single binding equilibrium. This broad distribution of trapping times would be expected to lead to an increased efficiency of trapping (see the Appendix for a quantitative discussion of how the distribution of trapping times affects efficiency and selectivity in a minimal mechanism for internalization or analogous processes). The benefit of a broad distribution of trapping times would be especially large if internalization of cargo can be viewed as a kinetic proofreading process, in which a delay between binding and a chemical step allows incorrect substrates to dissociate before being processed. This might be the case if chemically irreversible steps (such as GTP hydrolysis from the basal GTPase activity of dynamin) precede vesiculation. Kinetic proofreading has been proposed for processes such as protein synthesis, DNA replication, and T cell activation (*60*, *61*). Processes exhibiting stretched exponential pdfs for dissociation might help improve the efficiency of kinetic proofreading in cases where the correct substrate for the process frequently exhibits rapid dissociation from the reactive component.

It remains to be seen whether similar mechanisms might be observed for other processes in cell biology. However, dynamic interactions (i.e., interactions with high dissociation rates) appear to be important in many biological processes, including formation of an "immunological synapse" between a T cell and an antigen-presenting cell (*62*), targeting of Golgi membrane proteins (*63*), and binding of the glucocorticoid receptor to target genes (*64*). In cases where multiple proteins with multiple accessible conformations can interact in a spatially heterogeneous environment, the scale-free kinetics frequently observed in condensed matter physics may turn out to be important for understanding how biochemical reactions function in a biological context.

ACKNOWLEDGMENT

Xavier Michalet is acknowledged for generous help with the LabView programming and data analysis. We thank Prof. Henry Bourne and Dr. Guy Servant for the gift of the C5aR−EGFP plasmid and for helpful discussions. We thank the Margaret and H. A. Rey Laboratory for Nonlinear Dynamics in Medicine for providing the program dfa and useful information on the theory behind it.

APPENDIX

For processes in which a single binding reaction of a substrate leads to an irreversible reaction, and either a correct or incorrect substrate can react (Scheme 1) the probability

Scheme 1[a]

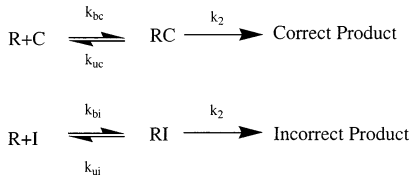

[a] R is a receptor, C a correctly targeted protein, and I an incorrectly targeted protein.

that a bound correct substrate will undergo the reaction is proportional to $\int_0^\infty e^{-k_{uc}t}\,dt$, with an analogous expression for the incorrect substrate. The fraction of incorrect product is given by k_{uc}/k_{ui} (assuming that k_{bc} and k_{bi} are identical, as would be the case for a diffusion-controlled reaction) (*60*). The difference in the unbinding rate constants can be expressed as a difference in free energy (since the binding rate constants are assumed to be equal). The relationship between this ΔG (expressed in units of kT) and the probability of a reaction occurring is plotted in Figure 2a of the Supporting Information (solid line).

We can also calculate the probability of the bound substrate undergoing the reaction for a scheme in which the dissociation of substrate has a stretched exponential pdf. In this case, the probability of the correct substrate undergoing reaction is proportional to $\int_0^\infty e^{-(k_{uc}t)^\beta}\,dt$ (*19*, *60*), with an analogous expression for the incorrect substrate. Here we assume that the binding energies are exponentially distributed, with β being the width of the distribution of binding energies (i.e., $\rho\Delta G$) and being equal to $\rho\ \exp(-\Delta G/kT_0, \beta = T/T_0)$ (*19*). At a given temperature T, one can express β in terms of kT, and determine the relationship between β and the relative probability of a substrate undergoing reaction (Figure 2a of the Supporting Information, dotted line).

As shown in Figure 2a of the Supporting Information, increasing the width of the binding energy distribution to $\sim 5kT$ (with a stretched exponential pdf) gives a relative probability of reaction similar to that predicted for increasing a single binding energy (ΔG) to $\sim 5kT$ (exponential pdf). In the limit of low binding energies and/or distribution widths, mechanisms with single binding energies are predicted to be more efficient, while in the limit of high binding energies and/or distribution widths, mechanisms with a distribution of energies are predicted to be more efficient. A distribution of energies $\sim 5kT$ in breadth would correspond in the model of Scheme 1 to a distribution of dissociation rate constants of ~ 2 orders of magnitude, which would not be physically unreasonable in a heterogeneous environment and has even been reported for a single enzymatic conformational change (*58*). This analysis suggests that mechanisms in which discrimination between substrates derives from differences in breadths of energy distributions for substrate binding can exhibit efficiencies comparable to those of more familiar mechanisms in which discrimination derives from differences in magnitudes of binding energies. In addition, this analysis suggests that the observation in this work of kinetics of receptor transport exhibiting no characteristic time scale over at least 2 orders of magnitude is consistent with a process having a binding energy distribution broad enough to produce a significant increase in the efficiency of internalization.

For a mechanism involving kinetic proofreading, a mechanism with a distribution of binding energies has even greater potential advantages for reaction efficiency and selectivity. Here, following the analysis of Hopfield (*60*), the probability of reaction for a kinetic proofreading reaction with a single binding energy is proportional to $\int_0^\infty e^{-k_{uc}t}\,k_2(t)\,dt$ (since the irreversible reaction involved in kinetic proofreading serves to make the rate constant for the chemical reaction step effectively time-dependent). The relative probability of reaction as a function of free energy difference for this mechanism is plotted in Figure 2b of the Supporting Information (solid line), using $k_2(t) = t$. Similarly, the probability of reaction for an analogous process with a distribution of binding energies would be proportional to $\int_0^\infty e^{-(k_{uc}t)^\beta}\,k_2(t)\,dt$ (Figure 2b of the Supporting Information, dashed line). In this case, at binding energies and/or distribution widths of more than $\sim 3kT$, the mechanism with a distribution of binding energies is predicted to be more efficient that the analogous single-binding energy mechanism, with a difference of many orders of magnitude in the limit of high binding energies and/or distribution widths. In addition, when the kinetic proofreading mechanism is compared to the mechanism of Scheme 1, the presence of a distribution of binding energies is predicted to lead to a larger relative benefit from kinetic proofreading than would be expected from a single binding energy (Figure 2c of the Supporting Information).

Of course, increasing the binding energy and increasing the width of a binding energy distribution are not necessarily mutually exclusive evolutionary strategies. It is also unclear which strategy would be easier to accomplish, for example, whether a given number of point mutations in a protein could make a larger change in the binding energy or in the distribution of binding energies. However, the above analysis does suggest that increasing the width of binding energy distributions (whether by mutations in a single protein or by targeting a heterogeneous array of binding proteins to a cellular structure) is a feasible strategy for increasing the efficiency of processes such as endocytosis of targeted receptors. In addition, it suggests that for kinetic proofreading processes, there might be a large selective advantage in optimizing the breadth of a binding energy distribution and that, conversely, for processes in which discrimination between substrates occurs on the basis of a difference in breadth of binding energy distribution, there might be a large selective advantage to introducing kinetic proofreading. It remains to be seen whether clathrin-mediated endocytosis actually employs a kinetic proofreading mechanism.

SUPPORTING INFORMATION AVAILABLE

Fluorescence time traces used for FCS (Figure 1), relative probabilities of reaction (Figure 2), and movies illustrating the effect of C5a on the mobility of the C5a receptors. The movies show a cell immediately before and ~5 min after addition of 10 nM C5a. Addition of C5a leads to clustering of C5aR in clathrin-coated pits (immobile) and subsequent internalization in clathrin-coated vesicles (highly mobile). The movies are speeded up by factor of 3; the frame rate was 10 frames/s. This material is available free of charge via the Internet at http://pubs.acs.org.

REFERENCES

1. Schmid, S. L. (1997) *Annu. Rev. Biochem. 66*, 511−548.
2. Kirchhausen, T. (1999) *Annu. Rev. Cell Dev. Biol. 15*, 709−732.
3. Gaidarov, I., Santini, F., Warren, R. A., and Keen, J. H. (1999) *Nat. Cell Biol. 1*, 1−7.
4. Miller, K., Shipman, M., Trowbridge, I. S., and Hopkins, C. R. (1991) *Cell 65*, 621−632.
5. Wiley, H. S., and Cunningham, D. D. (1982) *J. Biol. Chem. 257*, 4222−4229.
6. Moore, R. H., Hall, H. S., Rosenfeld, J. L., Dai, W. P., and Knoll, B. J. (1999) *Eur. J. Pharmacol. 369*, 113−123.
7. Zwart, D. E., Brewer, C. B., Lazarovits, J., Henis, Y. I., and Roth, M. G. (1996) *J. Biol. Chem. 271*, 907−917.
8. Orci, L., Carpentier, J. L., Perrelet, A., Anderson, R. G., Goldstein, J. L., and Brown, M. S. (1978) *Exp. Cell Res. 113*, 1−13.
9. Fire, E., Zwart, D. E., Roth, M. G., and Henis, Y. I. (1991) *J. Cell Biol. 115*, 1585−1594.
10. Barak, L. S., Ferguson, S. S. G., Zhang, J., Martenson, C., Meyer, T., and Caron, M. G. (1997) *Mol. Pharmacol. 51*, 177−184.
11. Goldstein, B., Wofsy, C., and Bell, G. (1981) *Proc. Natl. Acad. Sci. U.S.A. 78*, 5695−5698.
12. Katzir, Z., Nardi, N., Geffen, I., Fuhrer, C., and Henis, Y. I. (1994) *J. Biol. Chem. 269*, 21568−21575.
13. Umenishi, F., Verbavatz, J. M., and Verkman, A. S. (2000) *Biophys. J. 78*, 1024−1035.
14. Gilboa, L., Benlevy, R., Yarden, Y., and Henis, Y. I. (1995) *J. Biol. Chem. 270*, 7061−7067.
15. Fire, E., Gutman, O., Roth, M. G., and Henis, Y. I. (1995) *J. Biol. Chem. 270*, 21075−21081.
16. Petrelli, A., Gilestro, G. F., Lanzardo, S., Comoglio, P. M., Migone, N., and Giordano, S. (2002) *Nature 416*, 187−190.
17. Farsad, K., Ringstad, N., Takei, K., Floyd, S. R., Rose, K., and De Camilli, P. (2001) *J. Cell Biol. 155*, 193−200.
18. Schmidt, A., Wolde, M., Thiele, C., Fest, W., Kratzin, H., Podtelejnikov, A. V., Witke, W., Huttner, W. B., and Soling, H. D. (1999) *Nature 401*, 133−141.
19. Scher, H. (1991) *Phys. Today*, 26−34.
20. Pfister, G., and Scher, H. (1978) *Adv. Phys. 27*, 747.
21. Nagle, J. F. (1992) *Biophys. J. 63*, 366−370.
22. Axelrod, D. (2001) *Traffic 2*, 764−774.
23. Naik, N., Giannini, E., Brouchon, L., and Boulay, F. (1997) *J. Cell Sci. 110*, 2381−2390.
24. Wilde, M. W., Carlson, K. E., Manning, D. R., and Zigmond, S. H. (1989) *J. Biol. Chem. 264*, 190−196.
25. Servant, G., Weiner, O. D., Neptune, E. R., Sedat, J. W., and Bourne, H. R. (1999) *Mol. Biol. Cell 10*, 1163−1178.
26. Hansen, S. H., Sandvig, K., and van Deurs, B. (1993) *J. Cell Biol. 121*, 61−72.
27. Schwille, P., Korlach, J., and Webb, W. W. (1999) *Cytometry 36*, 176−182.
28. Schwille, P., Kummer, S., Heikal, A. A., Moerner, W. E., and Webb, W. W. (2000) *Proc. Natl. Acad. Sci. U.S.A. 97*, 151−156.
29. Steyer, J. A., Horstmann, H., and Almers, W. (1997) *Nature 388*, 474−478.
30. Funatsu, T., Harada, Y., Tokunaga, M., Saito, K., and Yanagida, T. (1995) *Nature 374*, 555−559.
31. Axelrod, D. (1989) *Methods Cell Biol. 30*, 245−270.
32. Stanley, H. E., Buldyrev, S. V., Goldberger, A. L., Havlin, S., Mantegna, R. N., Peng, C. K., and Simons, M. (1994) *Nuovo Cimento Soc. Ital. Fis., D 16*, 1339−1356.
33. Hoop, B., and Peng, C. K. (2000) *J. Membr. Biol. 177*, 177−185.
34. Buldyrev, S. V., Goldberger, A. L., Havlin, S., Mantegna, R. N., Matsa, M. E., Peng, C. K., Simons, M., and Stanley, H. E. (1995) *Phys. Rev. E 51*, 5084−5091.
35. Peng, C. K., Buldyrev, S. V., Havlin, S., Simons, M., Stanley, H. E., and Goldberger, A. L. (1994) *Phys. Rev. E 49*, 1685−1689.
36. Heneghan, C., and McDarby, G. (2000) *Phys. Rev. E 62*, 6103−6110.
37. Neher, E., and Stevens, C. F. (1977) *Annu. Rev. Biophys. Bioeng. 6*, 345−381.
38. Widengren, J., and Rigler, R. (1998) *Cell. Mol. Biol. 44*, 857−879.
39. Brock, R., and Jovin, T. M. (1998) *Cell. Mol. Biol. 44*, 847−856.
40. Neptune, E. R., and Bourne, H. R. (1997) *Proc. Natl. Acad. Sci. U.S.A. 94*, 14489−14494.
41. Korlach, J., Schwille, P., Webb, W. W., and Feigenson, G. W. (1999) *Proc. Natl. Acad. Sci. U.S.A. 96*, 9966.
42. Hansen, S. H., Sandvig, K., and van Deurs, B. (1993) *J. Cell Biol. 121*, 61−72.
43. Heuser, J. (1980) *J. Cell Biol. 84*, 560−583.
44. Sever, S., Damke, H., and Schmid, S. L. (2000) *J. Cell Biol. 150*, 1137−1147.
45. Sheets, E. D., Lee, G. M., Simson, R., and Jacobson, K. (1997) *Biochemistry 36*, 12449−12458.
46. Edidin, M., and Stroynowski, I. (1991) *J. Cell Biol. 112*, 1143−1150.
47. Elson, E. L., and Reidler, J. A. (1979) *J. Supramol. Struct. 12*, 481−489.
48. Bouchard, J.-P., and Georges, A. (1990) *Phys. Rep. 195*, 127−293.
49. Gilbert, T. L., Bennett, T. A., Maestas, D. C., Cimino, D. F., and Prossnitz, E. R. (2001) *Biochemistry 40*, 3467−3475.
50. Bereiter-Hahn, J., Fox, C. H., and Thorell, B. (1979) *J. Cell Biol. 82*, 767−779.
51. Damke, H., Binns, D. D., Ueda, H., Schmid, S. L., and Baba, T. (2001) *Mol. Biol. Cell 12*, 2578−2589.
52. Brown, C. M., and Petersen, N. O. (1998) *J. Cell Sci. 111*, 271−281.
53. Nossal, R. (2001) *Traffic 2*, 138−147.
54. Chou, T., Kim, K. S., and Oster, G. (2001) *Biophys. J. 80*, 1075−1087.
55. Schmid, S. L., and Carter, L. L. (1990) *J. Cell Biol. 111*, 2307−2318.
56. Frauenfelder, H., Sligar, S. G., and Wolynes, P. G. (1991) *Science 254*, 1598−1603.
57. Wennmalm, S., Edman, L., and Rigler, R. (1999) *Chem. Phys. 247*, 61−67.
58. Edman, L., Foldes-Papp, Z., Wennmalm, S., and Rigler, R. (1999) *Chem. Phys. 247*, 11−22.
59. Lu, H. P., Xun, L. Y., and Xie, X. S. (1998) *Science 282*, 1877−1882.
60. Hopfield, J. J. (1974) *Proc. Natl. Acad. Sci. U.S.A. 71*, 4135−4139.
61. McKeithan, T. W. (1995) *Proc. Natl. Acad. Sci. U.S.A. 92*, 5042−5046.
62. Grakoui, A., Bromley, S. K., Sumen, C., Davis, M. M., Shaw, A. S., Allen, P. M., and Dustin, M. L. (1999) *Science 285*, 221−227.
63. Cole, N. B., Smith, C. L., Sciaky, N., Terasaki, M., Edidin, M., and Lippincott-Schwartz, J. (1996) *Science 273*, 797−801.
64. McNally, J. G., Muller, W. G., Walker, D., Wolford, R., and Hager, G. L. (2000) *Science 287*, 1262−1265.

BI026059V